Welding in the World (2023) 67:1049–1057
https://doi.org/10.1007/s40194-023-01510-w

RESEARCH PAPER

Alloy modification for additive manufactured Ni alloy components—part I: effect on microstructure and hardness of Invar alloy

Antonia Eissel[1] · Lorenz Engelking[2] · René Gustus[3] · Kai Treutler[1,3] · Volker Wesling[1] · Dirk Schroepfer[2] · Thomas Kannengiesser[2]

Received: 3 October 2022 / Accepted: 1 March 2023 / Published online: 11 March 2023

Abstract
Alloy 36 (1.3912), also known as "Invar," is an alloy with 36% nickel. The alloy has a remarkably low thermal expansion coefficient in certain temperature ranges. This peculiarity is called the invar effect, which was discovered in 1896 by the Swiss physicist Charles Édouard Guillaume Sahoo and Medicherla Mater today Proc 43:2242-2244, (2021). Therefore, it is used in applications in which dimensional stability is critical, such as molding tools for composite materials in aerospace, automotive applications, or liquified natural gas (LNG) cargo tanks. Moreover, increasingly complex structures and the optimization of resource efficiency also require additive manufacturing steps for the production or repair of components Frazier J Mater Eng Perform 23:1917-1928, (2014); Treutler and Westling, (2021). Additively manufactured components have a heterogeneous microstructure and anisotropic mechanical properties Guévenoux et al. (2020). In addition, the manufactured components require subsequent machining surface finishing, like finish milling, to achieve their final contour. Nickel iron alloys are difficult to machine Zheng et al. Adv Mater Res 988:296–299, (2014). Additionally, inhomogeneous microstructure may lead to unstable cutting forces and conditions. In part I of this investigation, the initial alloy 36 is modified with the elements Ti, Zr, and Hf up to a maximum of 0.33 wt.-%. The influence of the modification elements on the microstructure as well as on the hardness of the AM components is examined. Furthermore, one modification is applied to metal arc welding process and investigated. Part II focuses on the effect of the alloy modifications on machinability as well as on the surface integrity of plasma-transferred-arc-welded (PTA) and finish milled invar components.

Keywords Modification of structural morphology · Fe–Ni-alloy · Plasma transferred arc welding

1 Introduction

Alloy 36 is also known as "Invar" and is continuously developed due to its special properties. This characteristic is the remarkably low coefficient of thermal expansion below the Curie temperature [1, 2]. As a result, the Fe–Ni alloy is used when excellent dimensional stability over a wide temperature range is required, such as in high-reliability structural material for cryogenic liquid storage and transport and composite molds for aerospace applications [3–6]. Furthermore, the high nickel content increases the corrosive resistance of the alloy compared to carbon steels [6]. As a result of the growing efforts for efficient use of energy, raw materials, and resources, more complex structures and component repair are preferred. Additive manufacturing is particularly ideal for this purpose [7, 8]. However, additively manufactured components have an anisotropic and heterogeneous

Recommended for publication by Commission II - Arc Welding and Filler Metals

✉ Antonia Eissel
antonia.eissel@tu-clausthal.de

✉ Lorenz Engelking
lorenz.engelking@bam.de

[1] Institute of Welding and Machining (ISAF), Agricolastr. 2, 38678 Clausthal-Zellerfeld, Germany

[2] Federal Insitute for Material Research and Testing (BAM), Unter Den Eichen 87, 12205 Berlin, Germany

[3] Clausthal Centre for Material Technology, Agricolastr. 2, 38678 Clausthal-Zellerfeld, Germany

microstructure. The components also require subsequent surface machining in order to realize the tolerance specification and high safety requirements for the surface integrity [9, 10]. Determinants of surface integrity include metallurgical (e.g., surface microstructure), topological (e.g., surface defects, roughness), and mechanical (e.g., residual stresses) factors that are key to the safety and performance of the components [11]. Alloy 36 exhibits high ductility and low thermal conductivity, so the subsequent machining process should be optimized by modifying the microstructure. There are already studies on the modification of Alloy 36, but these are mostly based on experiments using induction melting furnace or vacuum arc melting furnaces [12–15]. In the studies, the elements Ti and Zr were added as refiners to the alloy and influenced the morphology of the microstructure. As a result, the columnar grain in the solidification structure became shorter and thinner. It was concluded that Ti and Zr have a grain refinement effect on the solidification structure of Fe-36Ni invar alloy. Moreover, there are no systematic studies for the effect of modified microstructure morphology on machining of Invar.

In part 1, alloy 36 is modified with Ti, Zr, and Hf at a maximum of 0.33 wt.-%. The elements are alloyed and welded using plasma transferred arc welding. Subsequently, the influence of the modification elements on the microstructure morphology and hardness is determined. In addition, the resulting precipitation is examined in detail. Additionally, one modification is transferred to metal arc welding using PVD coating on the solid wire (filler) and investigated. The microstructure of the weld metal and the coated weld metal is compared. Part II focuses on the effect of the alloy modifications on machinability as well as on the surface integrity of plasma-transferred-arc-welded (PTA) and finish milled components made of alloy 36.

2 Material and methods

2.1 Materials used

Alloy modifications were intended to the alloy 36, composed of 36% nickel and 64% iron, in order to realize a more homogeneous microstructure. For this purpose, Ti, Zr, and Hf were added according to a statistical experimental design, see Table 1, as these elements are supposed to have a positive effect on the microstructure morphology. The maximum addition of each element is 0.33 wt-%. Ti is known as a fine grain former and causes a further increase in strength through precipitation hardening as a result of carbide and nitride formation [16]. Likewise, Zr is considered a strong carbide former [17]. Hf has many identical chemical and physical properties to Zr. Nevertheless, there are differences between the two elements; for example, Hf has twice the density of Zr, which is why the effect of Hf on the alloy 36 was also being studied. The modification was achieved by adding the appropriate weight percentage and combination of the modifier elements in powder form, to the alloy 36 powder and mixed using a 3D shaking mixer TURBULA® by rotational and translational movements and inversion to guarantee a homogeneous distribution.

Table 1 Design of Experiments for alloy modifications

Exp	Ti (%)	Zr (%)	Hf (%)
0	-	-	-
1	0.33	-	-
2	-	0.33	-
3	-	-	0.33
4	0.1667	-	-
5	-	0.1667	-
6	-	-	0.1667
7	0.33	0.33	
8	0.33	-	0.33
9	-	0.33	0.33
10	0.33	0.33	0.33

2.1.1 Experimental setup

The alloy 36 welding experiments with and without modifiers were performed with a Plasma-Transferred-Arc welding system from Hettiger Schweißtechnik GmbH. Wall structures are welded by overlapping welding beads on substrates, i.e., one layer on top of the other in one direction applying a weave movement to achieve the required width. For the substrate, a sandblasted sheet with almost identical chemical composition to alloy 36 was selected as the substrate plate in order to minimize the accumulation of foreign elements. This contained minimal amounts of manganese and silicon. The interlayer temperature was less or equal to 150 °C while cooling. This was monitored and achieved tacticle by means of a thermocouple. All specimens were welded with argon. The welding current and welding voltage variables depending on the modification are listed in Table 2, as well as the other welding process influencing variables. As the modification elements have a higher melting point, the welding current and voltage had to be increased slightly. The criteria applied in this context were that the surface quality should be approximately the same for all walls.

2.1.2 PVD-coating

The modification that is most interesting in terms of cutting force in cooperation with part 2 is transferred to the gas metal arc welding process. The aim was the alloying of a wire filler of alloy 36 with 0.33 wt.-% Zr. This was realized by PVD process. For this purpose, the industry-standard

Table 2 Welding parameters for PTA process

	Welding gas	Welding current (A)	Welding voltage (V)	Welding speed (cm/min)	Width of pendulum (mm)	Intermediate layer temperature (°C)
FeNi36	Ar	180	21	20	18	150
Modifications	Ar	210	23	20	18	150

Table 3 Coating time and thickness, and element content

Element	Coating time in min	Coating thickness in µm	Zr in wt.-%
Zr	60	1.188	0.35

Fig. 1 PVD coating system with substrate electrode [19]

PVD system of Ceme-Con AG is used. The coating chamber, which is loaded with the substrate wire electrode in batches, can be seen in Fig. 1. On the right side are the metal targets, which is vaporized and thus coats the wire electrode. A detailed description of the coating process can be found in [18] (Table 3).

2.1.3 Metal arc welding

The metal arc welding process was carried out with a welding supply from EMW. This was automated using 3D-manufacture from HLT-Gulliver GmbH (Fig. 2). The parameters used for the uncoated and coated filler wire are shown in Table 4. As with PTA welding, welding was carried out only in one direction. Several weld beads were welded overlapping next to each other to achieve the desired width and then on top of each other to achieve the height. The interlayer temperature was determined on the basis of the plasma transferred arc process and also monitored and achieved tacticle by means of a thermocouple.

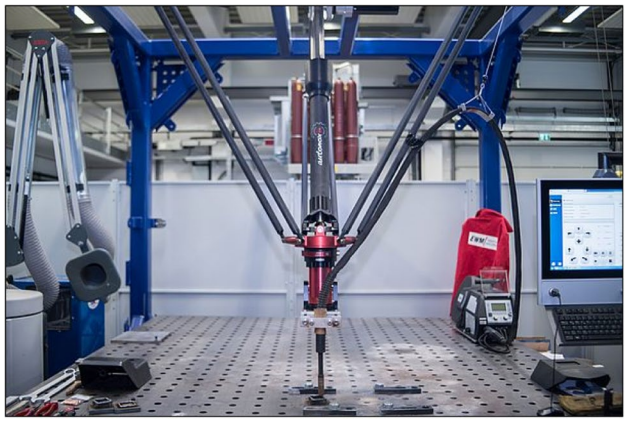

Fig. 2 Welding robot and welding power supply

Table 4 Welding parameters for GMAW process

Substrate	Invar
Shielding gas	M21/82% Ar + 18% CO_2
Wire feed	4,5 m/min
Travel speed	30 cm/min
Interlayer temperature	≤ 150 °C

2.1.4 Metallurgical analysis and hardness measurements

In order to perform the metallographic investigations and hardness measurements, a cross-section was cut from the wall structure by wire erosion. The specimens were embedded, ground, and polished for the light microscopic images. For a sufficiently high contrast ratio of the microstructure images, the specimens welded by PTA were etched for approx. 5 s with cold Adler. The specimens welded by GMAW were etched for approx. 20 s with Beraha II [20]. The Leica CRT 6 LED light microscope was used for light microscopic imaging. A field electron microscope model Nanolab 600 from FEI was used to determine the precipitation that occurs. The DuroScan G5 series hardness testing machine was used for the hardness measurement. Five measurements with HV 10 at different locations of the cross-section, four at the edge region of the specimen and one in the center of the cross-section, were made for the initial alloy and each modification of Table 1, shown as an example in Fig. 3.

3 Results and discussion

3.1 Microstructure analysis

Figure 4 shows the microstructure of the initial alloy and Fig. 5 shows exemplary three modifications with two different magnifications. The initial alloy exhibits an austenitic structure with unequal axis grains grown almost parallel to the direction of build-up. In the region of the contact zone between the layers, unmelted iron powder is present. This was etched more intensely than the rest of the microstructure by the Adler etching process (Fig. 4, b) and appears black at a scale of 200 µm (Fig. 2, a). Precipitates and small pores can be seen in the austenite grains (Fig. 4, c).

The modifications have almost identical microstructures as the initial alloy and thus have no significant influence. In addition, the modifications containing combination of elements showed the same behavior regarding the microstructure. Several reasons may explain the fact that the microstructure was not refined. On the one hand, the solidification phase in the welding process is considerably faster than in the melting furnace as described in [12–15], which meant that the refiner elements did not have enough time to react with alloy 36 and thus cannot contribute to grain refinement. On the other hand, the solubility of the modification elements at the selected content ranges is low even at near-equilibrium cooling. This could be the reason why the added elements precipitate in the grains of the austenite. However, [21] shows that a higher weight content of 1% of the elements Ti and Zr may lead to an increase in grain size.

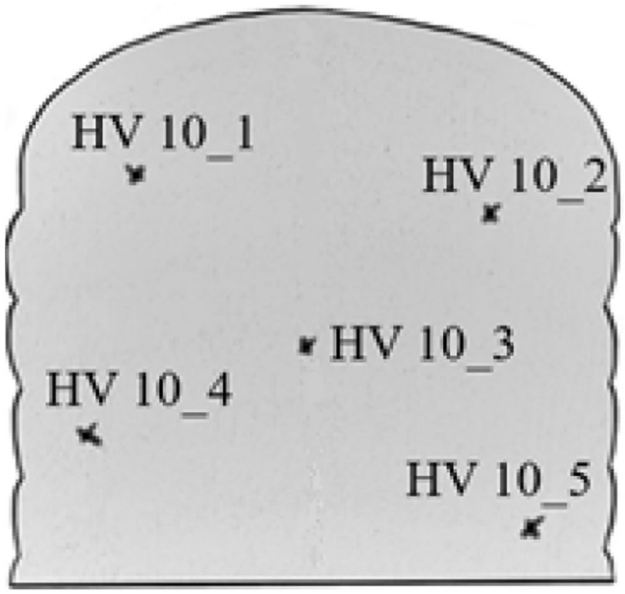

Fig. 3 Hardness measurement using the example of the upper layers

In the center of the sample, the length of the grains corresponds predominantly to the height of the layers (approx. 1–1.5 mm). However, there are also isolated cases of significantly longer grains growing over several layers with a size of up to 3 mm (see Fig. 6 marked blue). The width of the grains varies from 0.1 to 0.3 mm (in Fig. 6 marked in light blue).

In the initial alloy and all modifications, finely distributed minor precipitates and pores can be seen in all austenite grains. These are particularly well visible before etching of the specimen, as they appear bright (see Fig. 7, a). After etching, the precipitates appear in round or polyhedral form and are reflective (see Fig. 7, b). A further magnification of the occurring precipitates of the modifications in the microstructure can be seen in Fig. 5b, d, and f.

Some of the precipitates contain only particles of the modifying element and have an increased oxygen content (see Table 5). This can be attributed to the large surface area of the powder and an enrichment with oxygen during the mixing process. Furthermore, hexagonal grains also occur in the initial alloy and in the modifications that do not contain a modification element. Moreover, there are also round particles finely distributed in the microstructure that are only a few micrometers in size (Fig. 8, spectrum 5). These have the similar composition as the particles in the pores (see Table 5). The round pores, such as spectrum 3, can be attributed to gas inclusions. The

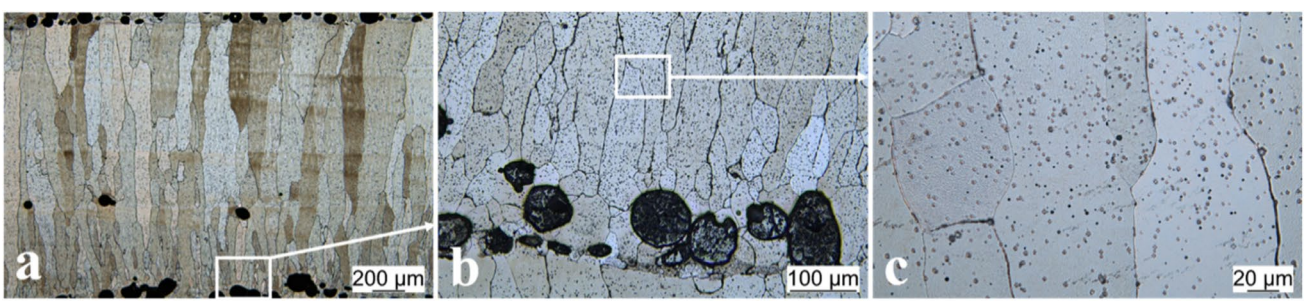

Fig. 4 Etched light microscopic images of microstructure of (**a**) Alloy 36, (**b**) detail of the interlayer area, and (**c**) magnification of the grains

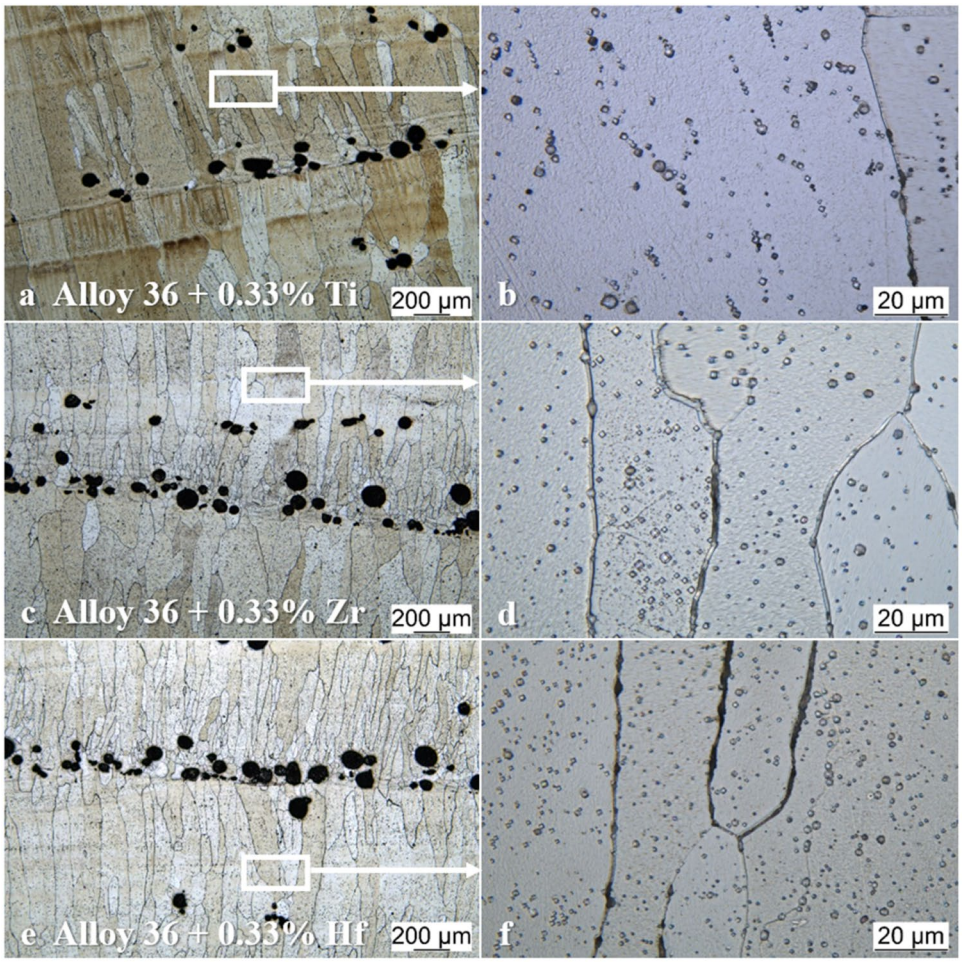

Fig. 5 Microstructure of **a** Alloy36 + 0.33 wt.-% Ti and detail **b**, **c**, Alloy 36 + 0.33 wt.-% Zr and detail, and **d**, **e**, Alloy 36 + 0.33 wt.-% Hf and detail **f**

gas, which has adhered to the powder during the mixing process, may have been degassed. In the polyhedral shapes, some of the precipitates may have been removed by the preparation of the sample, leaving only elemental particles to be located (see Fig. 8). This could also be the reason for the small residual particles of precipitate in the remaining cavity, see spectrum 1 and spectrum 4.

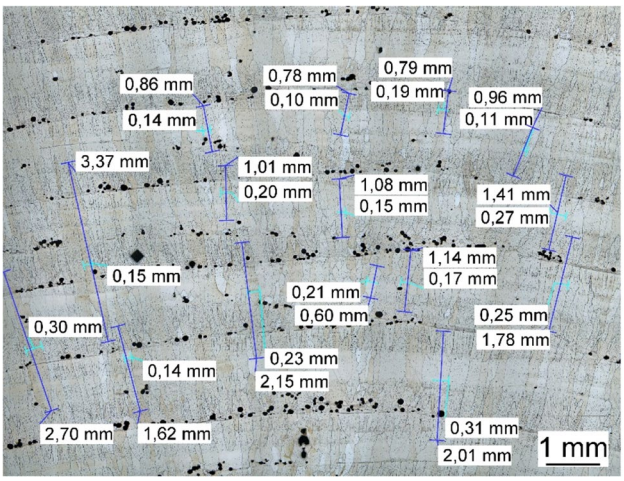

Fig. 6 Exemplary grain measurement of Alloy 36 + 0.33 wt.-% Ti

3.2 Microstructure analysis of metal arc weld

Figure 9a and c is the microstructures of the gas metal arc welded uncoated and coated solid wire filler of alloy 36. The morphology of the uncoated weld metal of alloy 36 is a combination of elongate cellular, small columnar, and regular cellular grains (see Fig. 9a). In addition, the microstructure is interspersed with round precipitates, which were intensively etched. In the modified alloy with approx. 0.33 wt.% Zr, dark precipitates no longer occur and the structure is entirely columnar dendritic. The microstructure can also be seen to have solidified in a significantly more directional shape (see Fig. 9c). Further magnification reveals a reticulation of finely dispersive and homogeneous precipitates at the grain boundaries (Fig. 9, d). These properties are assumed to result in better mechanical characteristics and machinability [22, 23].

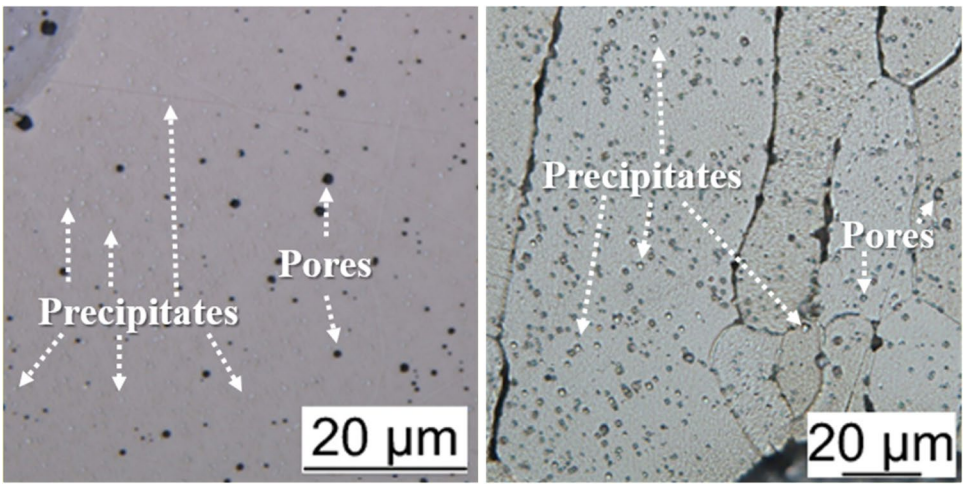

Fig. 7 Exemplary pores and precipitates in the microstructure of Alloy 36 + 0.33 wt.-% Hf: **a** unetched, **b** etched

Table 5 FESEM analysis of precipitations

	C	O	Fe	Ni	Ti	Zr	Hf
	At.-%						
Spectrum 1	3.9	48.2	36.6	1.6	9.7	-	-
Spectrum 2	3.4	2.3	63.0	31.2	-	-	-
Spectrum 3	17.6	58.0	2.4	0.5	-	20.2	-
Spectrum 4	4.2	26.3	16.2	16.2	-	-	4.2
Spectrum 5	10.7	53.6	14.5	-	-	19.2	-

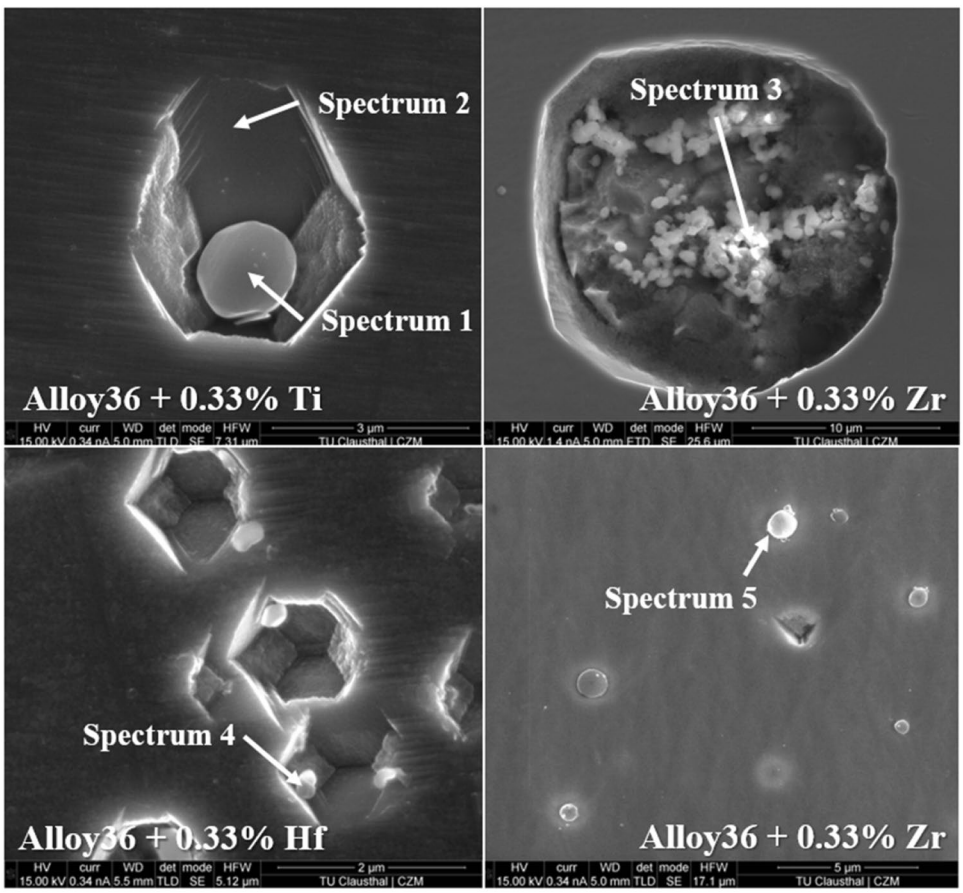

Fig. 8 Occurring precipitations of the modifications

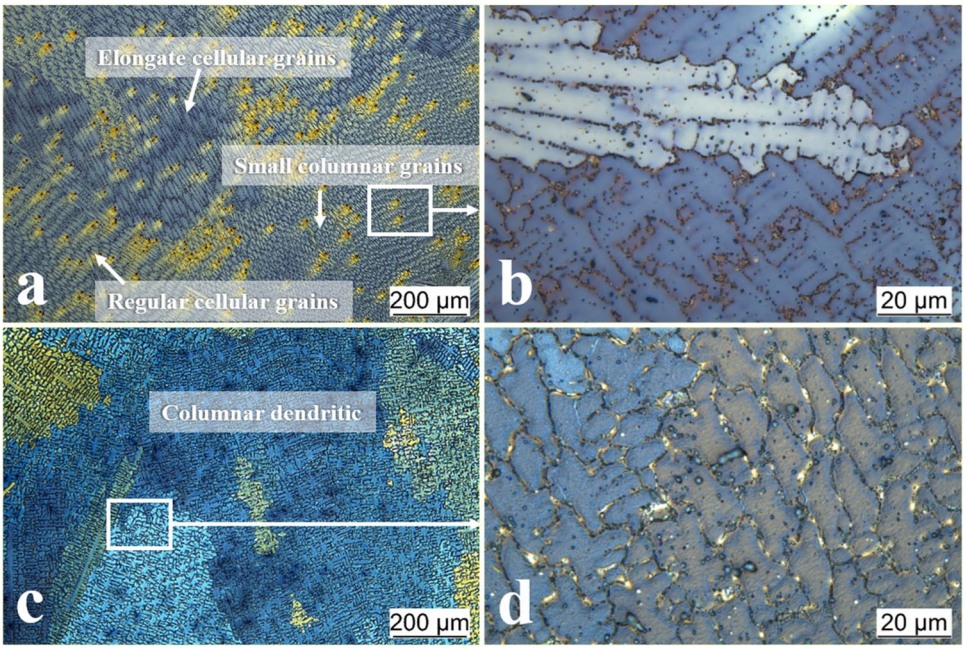

Fig. 9 Metal arc welded alloy 36 uncoated (**a** and **b**), and coated wire filler (**c** and **d**)

3.3 Hardness measurements

3.3.1 Hardness of PTA-welded specimens

Figure 10 illustrates contourplots of the average of the five individual hardness measurements (cf. Figure 3, HV 10) for the initial alloy and all modifications as a function of the alloy modification content. The hardness is more or less at a similar level, i.e., between 128 HV10 and 138 HV10. However, the modifications with different Zr or Hf contents show a slight increase in hardness. The modification with 0.33 wt.-% Hf has the highest hardness with 138 HV10. In contrast, the hardness of the modifications with pure Ti is minimally lower than of the initial alloy. When Ti is combined

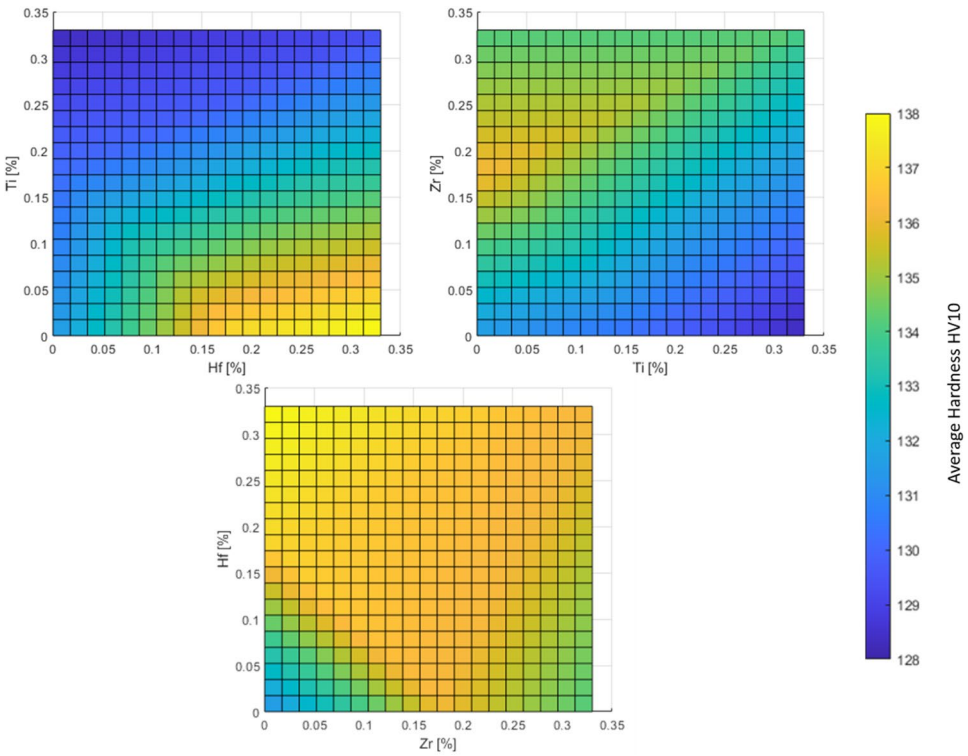

Fig. 10 Contour plots of average hardness of the five measurement points (according Fig. 1, HV 10) vs. the alloy modification content (Zr, Ti, Hf)

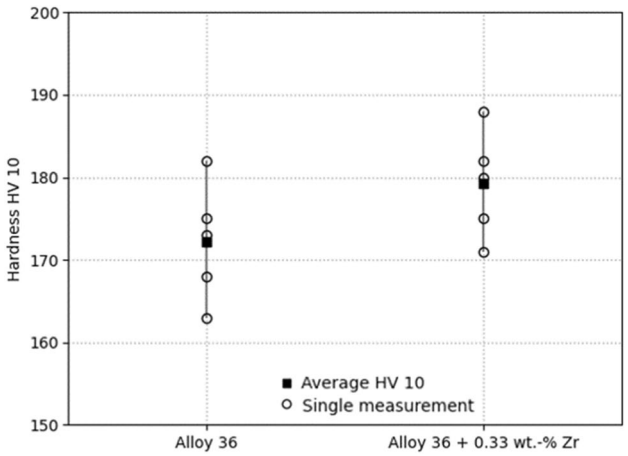

Fig. 11 Hardness measurement HV 10 of Alloy36 uncoated and coated filler wire

with Zr, a small hardness increase is observable. The slightly increased hardness values of only Zr and Hf can be related to the distribution of the precipitates. Zr and Hf precipitates occur uniformly distributed in the austenite grains, while the precipitates from Ti agglomerate to form lines (see Fig. 5b).

3.3.2 Hardness of GMAW-welded specimen

Figure 11 is a representation of the measured hardness values of the weld metal generated with uncoated and coated wire. The five individual measurements are plotted on top of each other and the average value formed is shown as a dark square. The coating of the wire with Zr leads to a slight increase in the average hardness HV 10, comparable to the hardness increase of PTA-welded specimens. Thus, the hardness of Alloy 36 is approx. 172 HV 10 and of Alloy 36 + 0.33 wt.-% Zr is approx. 180 HV 10. Accordingly, the modification with Zr and the resulting precipitates at the grain boundaries influence the hardness and lead to a slightly increased hardness.

4 Conclusion

Metallographic investigations and hardness measurements were carried out on the PTA-welded initial alloy, as well as on the modifications with Ti, Hf, and Zr up to a maximum of 0.33 wt.%. The main conclusions are the following:

(1) The microstructure of the initial alloy consists of unequal axis austenite, which means that the grains are significantly larger in the longitudinal direction than perpendicular to the direction of the structure (see Fig. 6).

(2) Neither the different weight percentages nor the combinations of elements show significant influence on the microstructure by PTA-welded. This is probably caused by the short solidification phase of the welding process.

(3) Finely distributed polyhedral and round precipitates are formed in the austenite grains. These contain particles of the modifying element.

(4) The coating of the filler wire clearly influences the morphology of the microstructure by GMAW. The microstructure of uncoated alloy 36 is composed of elongate cellular, small columnar, and regular cellular grains and the coated alloy 36 with approx. 0.33% Zr shows an entirely columnar dendritic structure.

(5) The hardness is only slightly influenced by the modification elements. A moderately positive influence can be seen by the elements Hf and Zr. The influence of Zr can be observed in both processes, PTA and GMAW welding. Especially in GMAW-welded microstructure, the increase in hardness is caused by a homogeneous distribution of precipitates at the grain boundaries.

Acknowledgements The IGF project IGF No. 20.979 N (DVS 01.3211) of the Research Association of the DVS was supported by the Federal Ministry for Economic Affairs and Climate Action by the AiF as part of the program for support of the cooperative industrial research (IGF) on the basis of a decision by the German Bundestag. We would like to thank for this funding and the companies involved in the project committee their support, in particular Deloro Wear Solutions GmbH, ECKART GmbH, and S3 Handel und Dienstleistungen UG for providing the welding powder, WOLF Werkzeugtechnologie GmbH for providing the milling tools, and DMG MORI Ultrasonic Lasertec GmbH for providing the ultrasonic actuator. We also thank Sabine Friederichs from ISAF for her support in the preparation of the microstructure and the hardness measurements.

Funding Open Access funding enabled and organized by Projekt DEAL. The IGF project IGF No. 20.979 N (DVS 01.3211) of the Research Association of the DVS was supported by the Federal Ministry for Economic Affairs and Climate Action by the AiF as part of the program for support of the cooperative industrial research (IGF) on the basis of a decision by the German Bundestag.

Declarations

Conflict of interest The authors declare no competing interests.

References

1. Shiga M (1996) Invar alloy. Current Opinion in Solid State and Materials Science 340–348. https://doi.org/10.1016/S1359-0286(96)80023-4
2. Liu HW, Sun ZH, Wang GK, Sun XR, Li JX, Xue F, Peng HF, Zhang YF (2016) Effect of aging on microstructures and properties of Mo-alloyed Fe-36Ni invar alloy. Mater Sci Eng 654:107–112. https://doi.org/10.1016/j.msea.2015.12.018
3. Saito H, Chikazumi S, Hirone T (1978) Physics and applications of invar alloys. Maruzen Company, LTD, Tokyo
4. Jasthi BJ, Arbegast WJ, Howard SM (2009) Thermal expansion coefficient and mechanical properties of friction stir welded Invar (Fe-36%Ni). J Mater Eng Perform 925–934. https://doi.org/10.1007/s11665-008-9320-7
5. Yingguang L, Nanya L Gao J (2014) Tooling design and microwave curing technologies for the manufacturing of fiber-reinforced polymer composites in aerospace applications. The International Journal of Advanced Manufacturing Technology 591–606. https://doi.org/10.1007/s00170-013-5268-3
6. Corbacho JL, Suárez JC, Molleda F (1998) Welding of invar Fe-36Ni alloy for tooling of composite materials. Welding Int 966–971. https://doi.org/10.1080/09507119809448543
7. Treutler KV (2021) Wesling, The current state of research of wire arc additive manufacturing (WAAM): a review, Applied Sciences 11(18)
8. Donghong D, Pan Z, Cuiuri D, Li H (2015) Wire-feed additive manufacturing of metal components: technologies, developments and future interests. Int J Adv Manuf Technol 465–481. https://doi.org/10.1007/s00170-015-7077-3
9. Schroepfer D, Treutler K, Boerner A, Gustus R, Kannengiesser T, Wesling V, Maus-Friedrichs W (2021) Surface finishing of hard-to-machine cladding alloys for highly stressed components. Int J Adv Manuf Technol 1427–1442. 1427–1442
10. Durul U, Tugrul O (2011) Machining induced surface integrity in titanium and nickel alloys: a review. Int J Machine Tools Manuf 250–280. https://doi.org/10.1016/j.ijmachtools.2010.11.003
11. Ulutan D, Ozel T (2011) Machining induced surface integrity in titanium and nickel alloys: a review. Int J Mach Tools Manuf 51(3):250–280. https://doi.org/10.1016/j.ijmachtools.2010.11.003
12. Abbasi SM, Morakabati M, Mahdavi R, Momeni A (2015) Effect of microalloying additions on the hot ductility of cast FeNi36. J Alloys Compounds 602–610. https://doi.org/10.1016/j.jallcom.2015.03.167
13. Cuixin C, Bin M, Baoxi L, Jun H, Haitao X, Yuqiang Z, Xuchen L (2019) Refinement mechanism and physical properties of arc melted invar alloy with different modifiers. Mater Chem Physics 138–147. https://doi.org/10.1016/j.matchemphys.2019.02.006
14. Yanchong Y, Weiqing C, Hongguang Z (2013) Effects of Ti-Ce refiners on solidification structure and hot ductility of Fe-36Ni invar alloy. J Rare Earths 927–932. https://doi.org/10.1016/S1002-0721(12)60381-0
15. Zheng, H-G, Yao LJ, Heng X (2013) Effect of two kinds of refiners on the solidification structure and property of invar alloy. High Temperature Materials and Processes 375–381. https://doi.org/10.1515/htmp-2012-0153
16. Schweißtechnische Fertigungsverfahren 2. Verhalten der Werkstoffe beim Schweißen. SpringerLink Bücher. Berlin, Heidelberg: Springer Berlin Heidelberg 2005
17 Arnold B, Zirkonium Z (2019) Zirkonia - ähnliche Namen, verschiedene Materialien. Springer, Berlin Heidelberg, Berlin, Heidelberg
18. Gehling T, Treutler K, Wesling V (2021) Development of surface coatings for high-strength low alloy steel filler wires and their effect on the weld metal microstructure and properties. Welding in the World 65:1591–1597. https://doi.org/10.1007/s40194-021-01086-3
19. Gehling T, Treutler K, Wesling V (2023) Wire electrode of 5754 aluminum modified by PVD-thin film depositions. Welding in the World. https://doi.org/10.1007/s40194-022-01435-w
20. Leistner E, Weck E (1982) Metallographische Anleitung zum Farbätzen nach dem Tauchverfahren, Teil 2: Farbätzmittel nach Beraha uund ihre Abwandlungen, vol Fachbuchreihe. Deutscher Verlag für Schweißtechnik, Schweißtechnik
21. Eissel A, Engelking L, Treutler K, Schroepfer D, Wesling V, Kannengiesser T (2021) Nickel-iron-alloy modification to enhance additively welded microstructure for subsequent milling. AJP 85–99. https://doi.org/10.1007/978-3-030-95463-5_6
22. Eissel A, Engelking L, Treutler K, Wesling V, Schröpfer D, Kannengießer T (2022) Modification of Co–Cr alloys to optimize additively welded microstructures and subsequent surface finishing. Welding in the World 66:2245–2257. https://doi.org/10.1007/s40194-022-01334-0
23. Engelking L, Schroepfer D, Kannengiesser T, Eissel A, Treutler K, Wesling V (2023) Alloy modification for additive manufactured Ni alloy components part II: effect on subsequent machining properties. Welding in the World. https://doi.org/10.1007/s40194-022-01438-7
24. Sahoo A, Medicherla VRR (2021) Fe-Ni Invar alloys: a review. Mater Today Proc 43:2242–2244. https://doi.org/10.1016/j.matpr.2020.12.527
25. Frazier WE (2014) Metal additive manufacturing: a review. J Mater Eng Perform 23:1917–1928. https://doi.org/10.1007/s11665-0140-0958-z
26. Guévenoux C, Hallais S, Charles A, Charkaluk EA (2020) Constantinescu: influence of interlayer dwell time on the microstructure of Inconel 718 Laser Cladded components. Optics & Laser Technol 128. https://doi.org/10.1016/j.optlastec.2020.106218
27. Zheng XW, Ying GF, Lu J, Yang NH, Chen Y, Fu YC (2014) The influence of cutting parameters on the cutting forces when milling Invar36. Adv Mater Res 988:296–299